



Digital twin for predictive maintenance on the Espartxo Bridge. Application to early detection of under-foundation scour

Javier Sánchez-Haro^{a,*}, Marianela García^b, Guillermo Capellán^b, Almudena da Costa^c, Paula Perez^a, Javier Añó^d

^a Structural department of University of Cantabria, Av. de los Castros 44, Santander 39005, Spain

^b Arenas&Asociados Ingeniería de Diseño S.L., Marques de la ensenada 11, Santander 39009, Spain

^c Department of Ground Engineering and Materials Science of University of Cantabria, Av. de los Castros 44, Santander 39005, Spain

^d FIA Ingenieros, Spain

ARTICLE INFO

Keywords:

Scour
Dynamic analysis
Soil-structure interaction
Digital twin
Predictive maintenance

ABSTRACT

This article describes the process of developing a digital twin aimed at being used for the predictive maintenance of scour on the Espartxo Bridge in San Sebastián, which is continuously monitored in real time. The main objectives of the research are to describe a methodology for creating the digital twin and to establish an effective strategy for the early identification of scour in bridge foundations, which pose a significant risk of structural damage. The developed methodology is based on hydraulic, geotechnical, and structural analyses, combining experimental tests on the bridge with the development of numerical models. As a result of the research, a bi-univocal correlation is established between the variation of a specific frequency and the depth of scour, and the analysis of horizontal vibration modes is determined to be an effective strategy for detecting scour.

1. Introduction

The probability of a bridge collapse is non-negligible, as indicated by various probabilistic studies based on available bridge data [1]. Scour around bridge piers is identified as the primary cause of structural failures in the majority of conducted studies; for instance, in the United States, scour is responsible for over 50 % of collapses [2]. It remains a significant factor even in countries with high seismic risk, such as Turkey [3]. Given its relevance, researchers have studied this phenomenon in recent years from various perspectives. Various theoretical formulations predicting scour in foundations have been proposed, and their results have been compared [4], revealing non-negligible differences among them. In fact, some authors have highlighted significant errors when using theoretical formulations [5,6]. For this reason, experimental models have been developed in controlled environments [7], establishing connections between scour and vibration frequency in isolated elements [8,9]. However, the challenge with these partial models is the lack of knowledge about the complete structure's impact, and additionally, the scale-changing factor of the real structure remains unknown.

For this reason, instrumentation in real bridges has been utilized as a

tool to detect scour through frequency variation [10,11]. There are different instrumentation techniques for detecting scour. Instrumentation with underwater sensors, such as electromagnetic ones [12], while expensive, may face operational issues due to impact from debris in the water channel [13]. Hence, it is quite common to analyze the frequencies and vibration modes of bridges using accelerometers [14]. Other monitoring variants include controlling environmental variables instead of structural ones [15], deploying special vehicles to monitor induced excitation on the bridge and analyze resulting scour [16], or even detecting scour through Bayesian techniques [17]. The arrangement of protective elements to reduce scour risk has also been analyzed [18,19]. Nevertheless, as of today, the assessment of bridge condition based on variation in vibration modes using numerical analysis continues to be a common practice [20]. This is due to the fact that prevention techniques are not sufficiently developed or implemented. Scour not only occurs during major flood events defined by return periods; some authors recommend probabilistic methods to account for the cumulative damage caused by a continuous process [21], especially in the presence of turbulent flow around the foundation [22]. This article presents a numerical analysis of the Espartxo Bridge based on continuous instrumentation data and real tests carried out on it. The goal is to

* Corresponding author.

E-mail address: sanchezja@usal.es (J. Sánchez-Haro).

generate a digital twin of the structure calibrated to account for the influence of the terrain on vibration frequencies. By doing so, with the bridge continuously monitored, a preventive alarm can be developed in case the specific variation in frequencies indicates the initiation of a scour process, whether caused by a 500-year return flood or by a cumulative process generated by turbulent flow around the piles.

2. Methodology

The general framework in which the research is conducted is described below, with the aim of establishing the general guidelines that the proposed methodology outlines for the detection of scour in real bridges through the study of dynamic behavior. The developed methodology establishes that this study should include at least six phases, which are described below. A real case study will then be presented to more clearly illustrate the six phases of the methodology: The Espartxo Bridge.

Phase 1: Preliminary Analysis. First, a preliminary analysis must be conducted that gathers all available information about both the structure under analysis and its surroundings and context. This preliminary information must cover at least three main areas: structural data, data on the terrain near the bridge, and hydraulic and hydrological data for the area. Regarding the structural part, the information should include the structural layout, geometry, materials, and construction process, as well as any major event that may have affected the structure during its service life. Regarding the ground data, it should contain sufficient information to establish both soil-structure interaction and the necessary data for hydraulic analysis. Finally, in the preliminary analysis, the hydraulic study must be undertaken to statistically establish the scour scenarios, i.e., the statistical probabilities of different scour depths occurring at the foundation. This hydraulic analysis is based, on one hand, on the data characterizing the terrain near the bridge, as mentioned earlier, and on the hydrological study that establishes the river's design floods according to the return period.

The ultimate goal of the process is to obtain a digital model that accurately reproduces the actual behavior of the bridge. This approach differs from the design phase, where calculations aim to leave a margin of safety. In this case, the goal is to reproduce the actual behavior of the bridge as accurately as possible, considering its true conditions. For this reason, it is crucial to have real test data on the bridge.

Phase 2: Bridge Testing. A suitable occasion to gather data on the actual behavior of the bridge is the tests conducted before the bridge is put into service, which are often mandatory. Typically, static tests are performed on road bridges, and both static and dynamic tests on railway bridges. However, as seen in the case presented, dynamic information is also important for road bridges. Since pre-service tests are not conducted with regular traffic, it is also essential to have information during the bridge's service life, i.e., with the usual loads the bridge carries. Whether during the pre-service tests or tests during the bridge's service life, this methodology strongly recommends conducting some kind of test that includes a horizontal load on the bridge. The idea behind this specific test is to study the horizontal restraint of the ground on the bridge. The real case presented in this article will demonstrate the importance of this test.

Phase 3: Finite Element Model. Once all the preliminary data have been gathered, and real tests have been conducted on the bridge to provide actual data, a finite element model must be developed. At this point, it is crucial that the model is created by personnel with extensive experience in this field. Creating a finite element model requires, contrary to common belief, significant reliance on the engineer in charge. The type of elements defined, connections between elements, materials, types of analysis, etc., and even the choice of software, can result in sufficiently different outcomes, potentially leading to an incorrect interpretation of the bridge's behavior.

Phase 4: Calibration of the Digital Model. Once the model is developed, it must be calibrated based on the real data obtained from tests on

the bridge. The parameters that must be selected for calibration depend on each case, but at a minimum, the modulus of elasticity of the materials, the density, and the stiffness of the supports should always be considered. It is recommended to first calibrate the static tests and then the dynamic ones. Static calibration involves fewer parameters than dynamic calibration, making it easier. Once these parameters are calibrated, it is recommended to calibrate the parameters that affect dynamic behavior under vertical loads. Finally, it is recommended to calibrate the parameters that affect dynamic behavior under horizontal loads, where the influence of horizontal ground restraint is greater. The idea behind this sequential calibration process is to isolate parameters so they can be calibrated almost individually, minimizing uncertainty regarding the influence of some parameters on others.

Phase 5: Numerical Analysis. Once the model is calibrated and the digital model is established, the numerical analysis using finite elements can be performed. The model is subjected to the scour scenarios obtained from the hydraulic model, and the variations in the dynamic behavior of the bridge are analyzed. The objective of this analysis is to find some relationship between the depth of the scour and the dynamic behavior of the bridge. Ideally, a one-to-one relationship between the two would be established, so that changes in dynamic behavior are solely attributed to scour and not to any other defect. It is not always possible to achieve this one-to-one relationship, as it depends on the bridge and the available data, but even in such cases, it is useful to know that scour is suspected, allowing for preventive measures to determine the actual cause of the anomalous behavior.

Phase 6: Conclusions. After the numerical analysis, the main findings that help determine the degree of scour based on the dynamic behavior of the bridge are summarized. The following section presents the application of this methodology to a real case: the Espartxo Bridge.

3. Preliminary analysis of Espartxo Bridge

3.1. Analysis of the structural solution

The Espartxo Bridge [23] over the Urumea River in San Sebastián, Spain, was designed by the company Arenas & Asociados and opened to traffic in 2020. The bridge consists of two spans, one measuring 42 m and the other 17.4 m. The two spans are separated by a roughly 6 m tall V-shaped concrete pier. The structural solution for the bridge includes two longitudinal metallic ribs and intermediate metallic ribs, spaced every 3 m, as illustrated in Fig. 1.

The longitudinal ribs protrude 117 cm above the road level and extend 75 cm below it. This design was conceived, on the one hand, to provide sufficient clearance for the hydraulic section and, on the other hand, to separate the central traffic zone (7 m) from the sidewalks, as illustrated in Fig. 2.

The bridge has two sidewalks with a width of 4.0 m downstream and



Fig. 1. Bottom perspective of Espartxo Bridge.



Fig. 2. Upper perspective of Espartxo Bridge.

2.5 m upstream, separated from the central vehicle passage zone in the shorter span. Each of the sidewalks is supported by an additional longitudinal rib. In the main span area, the total width of the deck (including roadway and sidewalks) is 15.30 m, as shown in Fig. 3.

Above the metal structure, the roadway is placed, consisting of a 21 cm concrete slab supported by the transverse ribs. The slab and the metal transverse beams are connected through connectors.

The V-shaped pier, as shown in Fig. 4, is composed of a metallic box-section core filled with concrete, attached to an upper crossbeam, also metallic, which acts as a diaphragm between the main ribs of the deck. The arms forming the metallic core are embedded in a volume of prestressed concrete that shapes the final body of the pier. Due to its much higher rigidity than the neoprene bearings supporting the bridge at the abutments, the pier is responsible for absorbing all the horizontal forces acting on the bridge. However, despite being outside the ordinary riverbed, the pier presents a potential risk of scour during a flood. For this reason, a hydraulic study was conducted to determine, based on the return period of the flood, the potential level of scour that could be reached. This study is detailed in section 2.3 of this document.

The pilecap, with a thickness of 1.3 m and dimensions of 8.80 m x 6.65 m, transfers loads through 8 concrete piles, each with a diameter of 1.25 m and a length of 19.5 m.

The main materials and their characteristics are summarized in the Table 1.

The construction process [23] of the bridge was defined by the need to minimize the impact on the river’s natural environment as much as possible and to maintain traffic flow during the demolition of the adjacent old bridge and the construction of the new one. This led to three distinct construction phases: first, the construction of the roadway of the new bridge, then the demolition of the old bridge, and finally, the construction of the pedestrian sidewalks on the new bridge. For the foundation work, a temporary peninsula was required, Fig. 5a. The placement of the longitudinal ribs was carried out using cranes, Fig. 5b, while the transverse ribs were welded to the longitudinal ones.

3.2. Geotechnical analysis

The ground on which the bridge is supported has been studied through three boreholes: S-01 (Abutment 2), S-02 (Pier), and S-03

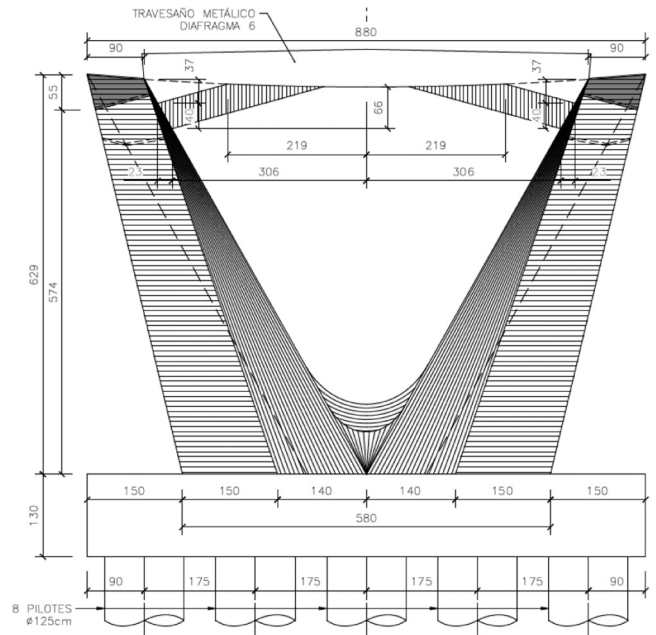


Fig. 4. V-shaped pier.

Table 1 Material description of Espartxo Bridge.

Element	Material	Description
Abutments	Concrete	HA-30/Pb/20/IIIb+Qb *
Piles	Concrete	HA-30/Pb/20/IIIb+Qb *
Pile cap	Concrete	HA-30/Pb/20/IIIb+Qb *
Pier	Concrete	HP-40/20IIIa*
Slab	Concrete	HA-30/Pb/20/IIIb+Qb *
Conc. Reinforcement	Steel	B-500S*
Connectors	Steel	St-37 **
Longitudinal Ribs	Steel	S 355 J0 *** for thickness < 13 mm S 355 J2 *** for thickness > 13 mm
Transversal Ribs	Steel	S 355 J0 *** for thickness < 13 mm S 355 J2 *** for thickness > 13 mm

*As per EHE
 ** As per DIN-17100
 *** As per Eurocode

(Abutment 1), located as illustrated in Fig. 6.

Standard penetration tests (SPT) were conducted at various depths during the borehole execution. A total of 14 samples were obtained: 3 from the SPT tests, 7 undisturbed (U) samples, and 4 paraffin-coated samples (P). Table 2 provides a summary of the conducted boreholes, including the SPT blow count (N) results, and the samples in which unconfined compression tests were done.

Fig. 7 displays the geotechnical profile beneath the bridge, derived from the interpretation of borehole data. As observed, the ground consists of a superficial layer of fill material overlying alluvial soils with

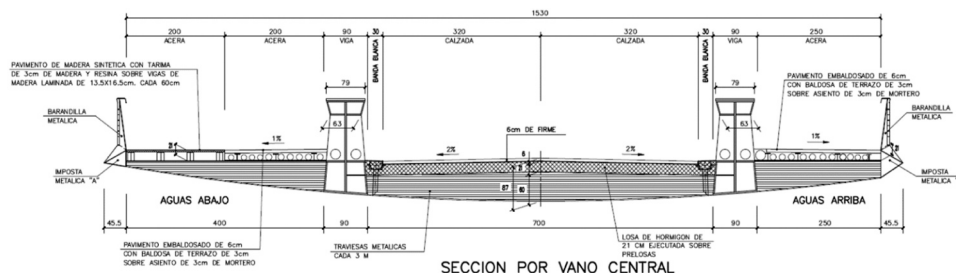


Fig. 3. Typical Cross section at main span.



a: Construction process. V shape Pier reinforcement.



b: Construction process. Longitudinal Rib placement.

Fig. 5. (a) Construction process.V shape Pier reinforcement. (b) Construction process. Longitudinal Rib placement.

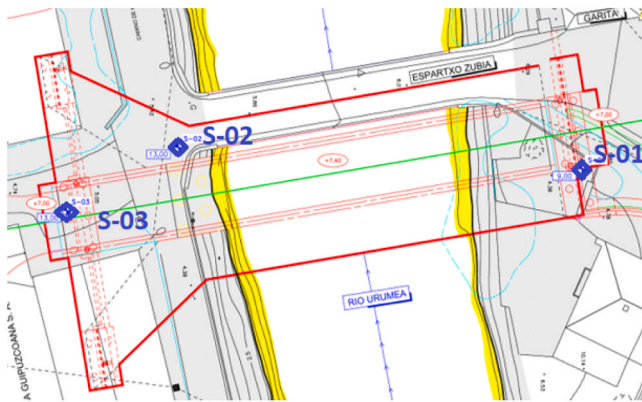


Fig. 6. Plan view location of the boreholes.

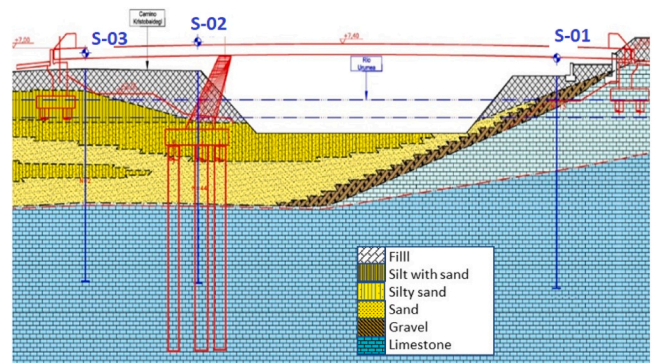


Fig. 7. Geotechnical soil profile under the bridge and Urumea river flow levels.

Table 2
Summary of the borehole's samples. Test values N_{SPT} .

Borehole	Depth (m)	Sample	N_{SPT}	Unconfined compression tests
S-01	3.00 – 3.50	SPT	13	
	6.50 – 6.75	U	50	
	13.81 – 14.00	P		X
	16.50 – 16.84	P		X
S-02	3.00 – 3.60	U	1	
	6.50 – 7.10	U	8	
	10.00 – 10.60	U	17	
	10.60 – 11.05	SPT	34	
S-03	3.00 – 3.60	U	4	
	6.50 – 7.10	U	6	
	10.00 – 10.60	U	6	
	10.60 – 11.05	SPT	2	
	13.50 – 13.60	P		X
	19.60 – 19.75	P		X

U: Undisturbed sample
P: Paraffin-coated core
SPT: Standard penetration test

variable thicknesses. Below the alluvial layers, the rock is encountered, characterized by a high degree of weathering and low values of Rock Quality Designation (RQD).

The superficial fill consists mainly of rocky material from excavation and alluvial sediments, comprising loose grey gravel with some clay and sand. Additionally, there is medium-consistency silty clay with sands and some gravel. The alluvial soil layer is composed of alternating

layers: i) silt with sand and some gravel, ii) silty sand with gravel, iii) sand with gravel, and iv) medium-density gravels. The rock, from the Lower Cretaceous period, consists of limestone with a highly weathered condition (Grade IV), characterized by extensive fracturing (RQD values below 20 %, even 10 %). This study focuses on the bridge pier as it receives the horizontal forces of the structure. Therefore, Fig. 8 provides a more detailed profile of the terrain in this area, corresponding to borehole S-02.

Geotechnical properties for the alluvial soil layers can be obtain from the results of the SPT tests. For the silty sand layer, blow counts are

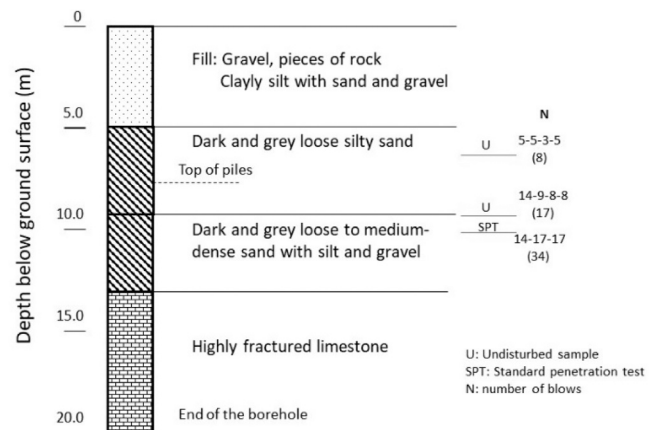


Fig. 8. Soil profile under the pier area (S-02).

available from undisturbed samples, one from borehole S-02 with a total of 8 blows, and another from S-03 with 6 blows. In the sand layer, a result of 17 blows was obtained from an undisturbed sample, and another of 34 from an SPT test, both values from borehole S-02.

Geotechnical properties for the highly fracture limestone can be obtained from the results of the unconfined compression tests that were done with samples prepared from blocks of the intact rock, and from the available values of the RQD (average 20 %, some values 10 %).

For the analysis presented in the following sections, it is necessary to estimate the value of the horizontal coefficient of subgrade reaction (K_h) for the strata in contact with the piles: layer 1: silty sand (1.5 m depth below the pilecap), layer 2: grey sand (4.5 m depth below the pilecap), and layer 3: limestone (highly fractured). As it is well known, there are different proposals by different authors to estimate this coefficient, but the Values always fall within a broad range but are sufficiently accurate for the calculations performed in the following sections.

In the following paragraphs, the method that was employed in this paper for this estimation is described for each layer of soil.

For the granular soils, the subgrade coefficient can be estimated from the blow count obtained in the SPT tests. This has been done for the layers of silty sand and sand.

As it is well known in geotechnical literature, there is a direct relationship between the blow count and the relative density of sands, as shown in Table 3.

According to the values of the number of blows of 6, 8 for the layer of silt sand and 17, 34 for the sand layer, loose and medium relative densities can be considered for each soil respectively.

Some of the proposals in the bibliography relate the horizontal coefficient of subgrade reaction with the relative density of sands. Classically Terzaghi [24], and more recently Reese [25], as shown in Fig. 9, present these relationships among the most commonly used.

In Fig. 9, it can be observed that the ranges for loose and medium dense are quite broad. In a slightly conservative manner, a relative density of 20 and another of 40 have been assumed within their respective ranges to consider values below the mean of both ranges in the calculations.

These values should be corrected according to the actual width of the piles (1.25 m). In addition, it has to be considered that K_h increases with depth in granular soils. For the layer of silty sand, with a thickness of 1.5 m, a constant and average value of K_h has been considered. For the sand layer, being thicker (4.5 m), an increasing law with depth has been considered.

Finally, the group effect between piles must be considered. According to Davis [26], Parkash [27], or Jampel [28], the value of K_h should be multiplied by a group factor (F_g) equal to 0.25 for separations lower to 3 times the diameter of the pile. The above three effects can be taken into account by using the well-known expression, Eq. 1:

$$K_h = \eta_h \frac{z}{D} F_g \tag{1}$$

where D is the diameter of the piles and z is the depth.

For the limestone, the estimation for K_h can be derived from the results of the unconfined compression tests and the RQD values. Cheng [29] proposed the following relationship between K_h and the modulus of deformation of the rock mass, E_m where the group factor has been added to obtain the commonly used expression:

Table 3
Relationship between the blow number and the relative density in granular soils.

No of blows	Relative density
5 –10	Loose
11 –30	Medium
31 –50	Dense
> 50	Very dense

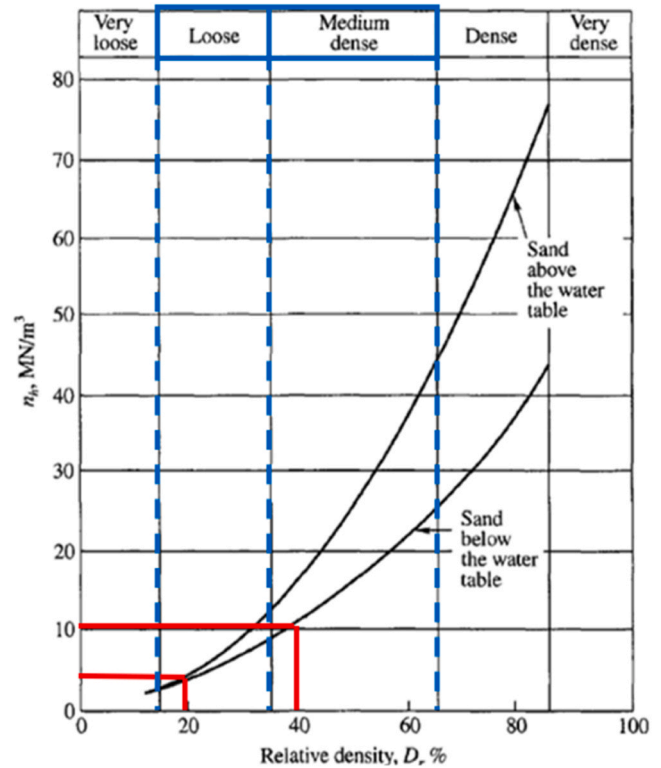


Fig. 9. Variation of η_h with the relative density of sands (Reese [25]).

$$K_h = \frac{A \cdot E_m}{D} F_g \tag{2}$$

where A is a coefficient that depends on the type of soil (3 for non-cohesive soils and 1,6 for cohesive soils), D is the diameter of the pile and F_g the group factor.

The value of E_m can be estimated from the results of the unconfined compression tests. In this case, the interpretation of the tests will give the modulus corresponding to the intact rock. The average obtain value is 2000 MPa. Just to obtain the value not for the intact rock but for the rock mass (RQD of 20 %), the proposal of Einstein [30] can be used. This

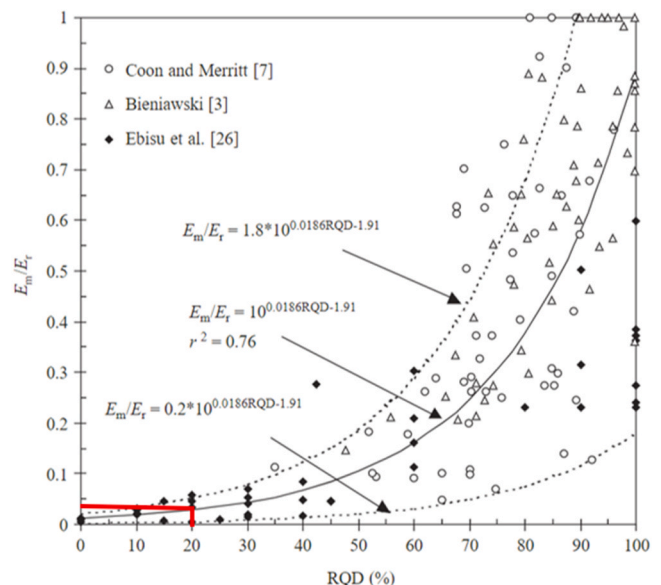


Fig. 10. Recommended relationship between RQD and E_m/E_r (Einstein [30]).

proposal is given in Fig. 10 where E_m is the modulus of the rock mass and E_r is the modulus of the intact rock.

The used value for calculations considering the Fig. 10 and the obtained value of module from the unconfined compression tests is equal to $E_m = 0.04 \times 2000 = 80 \text{ MPa}$.

In accordance with Eqs. 1 and 2 and the parameters explained earlier, the values of the subgrade reaction coefficient obtained for the profile generation are shown Table 4.

Due to the precision usually required in geotechnics, where relevant variations are typically at least an order of magnitude, the results of Eqs. 1 and 2 have been rounded to the nearest whole number in Table 4. At a depth of 1.5 m, where there are values for two different layers, the average between them has been used.

In Fig. 11, the law relating the horizontal coefficient of subgrade reaction to depth is observed according to the estimated values of Table 4 for the three layers described above.

3.3. Hydraulic analysis of torrential flows

Next, a hydraulic analysis is performed on the expected torrential flows in the design of the Espartxo Bridge to determine their impact on the terrain near the foundation of the V-shaped pier. Despite being separated as much as possible from the ordinary riverbed (Fig. 7), the V-shaped pier is at risk of being within the flood-prone zone depending on the considered design floods. Three design floods corresponding to return periods of 10 years (T10), 100 years (T100), and 500 years (T500) were provided by the administration that commissioned the project. For this research, these three floods were used as input data, Fig. 12.

Once the flow laws are defined as starting data, a hydraulic analysis is performed using the Mike 21 FM MT Mud Transport v2023 program. The design hydraulic parameters were estimated using this widely used software. Over 200 m of the Urumea River channel near the Espartxo Bridge is modelled, with the bridge located approximately in the middle of the modelled length. Regarding the roughness used in the flow, a Manning coefficient value of 0.03 was determined for both the centre of the channel and the margins. The model discretization is defined in three levels, Fig. 13a: a general mesh (2/3 length of the model approximately) to define bathymetry in the more distant areas (triangulated mesh with sides of approximately 4 m), a detailed mesh in the bridge area and its surroundings ((triangulated mesh with sides of approximately 1 m)), and a precision mesh in the foundation area of the V-shaped pier (triangulated mesh with sides of approximately 0.25 m), Fig. 13b. In the model, in addition to bathymetry provide by the administration that commissioned the project, the three terrain levels defined in Section 3.2 of this article have been incorporated, for instance, the density, granulometry data, etc., from on-site tests were applied in the model.

The inlet and outlet sections are defined at the beginning and end of the modelled bathymetry, where the design floods are to flow, as shown in Fig. 14. As boundary conditions, the design flood for each case (T10, T100, and T500) was imposed at the initial inlet section, while the outlet section was left free for the modelled bathymetry to determine the flow distribution.

The current velocities resulting from the model are analyzed in the vicinity of the piles of the Espartxo Bridge pier foundation for the three design floods, as shown in Fig. 15.

Table 4

Estimated calculation of the horizontal subgrade coefficient as per Eq. 1 and Eq. 2.

Layer	η_h (MN/m ³)	Z (m)	D (m)	F_g	K_h (kN/m ³)
silty sand	5.00	1.50	1.25	0.25	2000
sand	10.00	1.50	1.25	0.25	
sand	10.00	6.00	1.25	0.25	1000
	A	E_m (MPa)	D (m)	F_g	K_h (kN/m ³)
limestone	2.5	80	1.25	0.25	40000

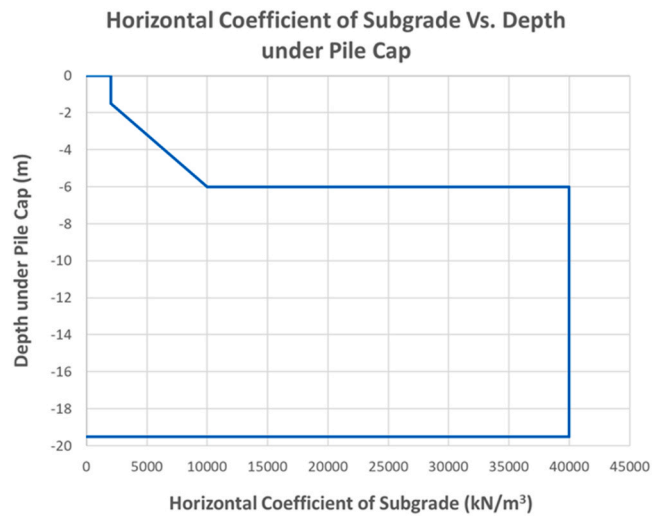


Fig. 11. Horizontal coefficient of subgrade Vs. Depth under pile cap.

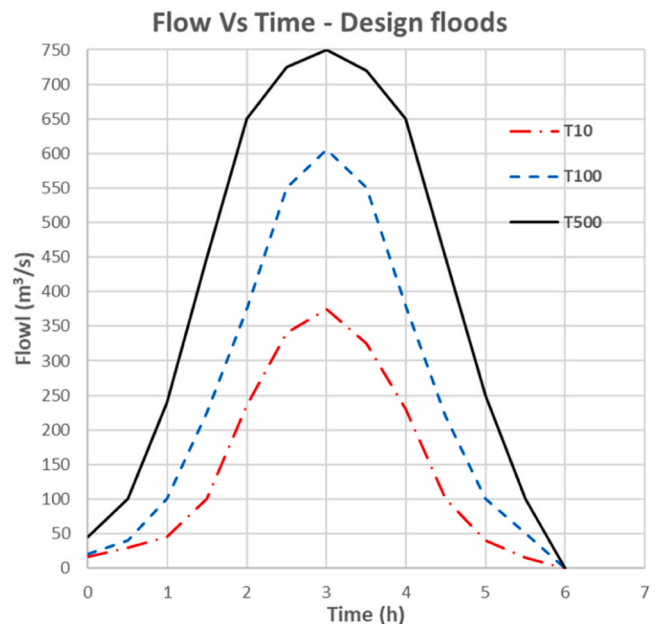


Fig. 12. Flow law for the design floods, T10, T100 and T 500.

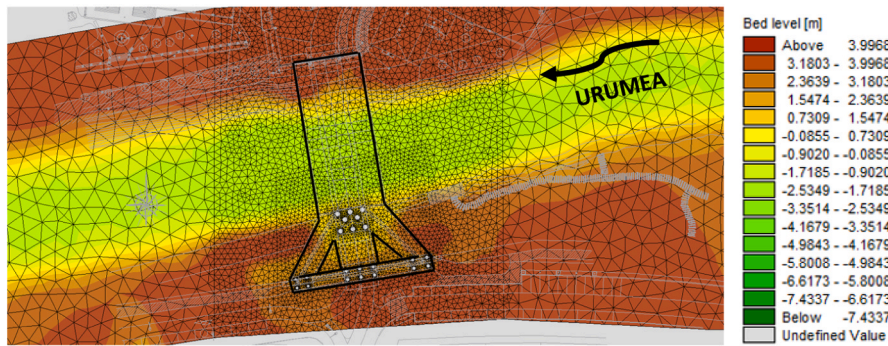
The model results confirm that the V-shaped pier is subject to scour processes, albeit to varying degrees, for the three design floods, as shown in Fig. 16. For the T10 flood, only the row of piles closest to the riverbed experiences significant scour. In the T100 flood, scour penetrates up to the middle row formed by the pair of piles. Finally, for the T500 flood, all the piles, to varying extents, undergo significant scour.

From the analysis of the entire hydraulic study, the maximum depth of scour for the 8 piles that make up the foundation of the V-shaped pier of the Espartxo Bridge is ultimately obtained, depending on the corresponding design flood, as shown in Fig. 17.

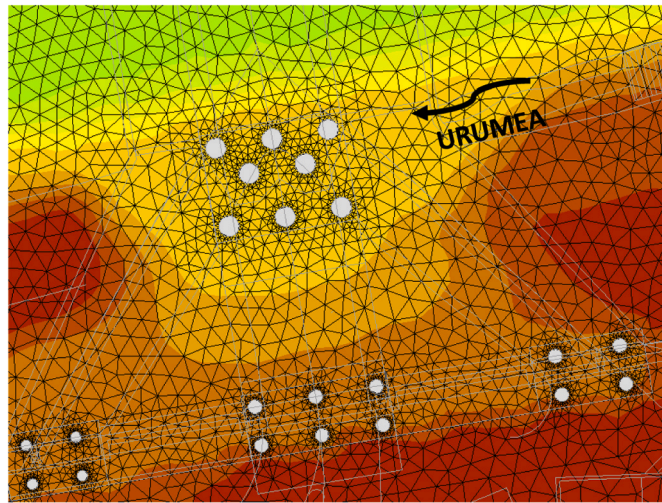
Based on this data, a structural analysis will be subsequently performed to study the impact of scour on the static and dynamic behaviour of the bridge.

4. Load test on Espartxo Bridge

On May 19, 2020, static and dynamic load tests were performed on the Espartxo Bridge over the Urumea River in San Sebastian, Spain, prior to open to traffic. Various sensors were placed along the bridge during



a: Bathymetry of the studied area model. Software Mike 21 FMN MT Mud Transp.v2023.



b: Detailed mesh. Software Mike 21 FMN MT Mud Transp.v2023

Fig. 13. (a) Bathymetry of the studied area model. Software Mike 21 FMN MT Mud Transp.v2023. Fig. 13b: Detailed mesh. Software Mike 21 FMN MT Mud Transp.v2023.

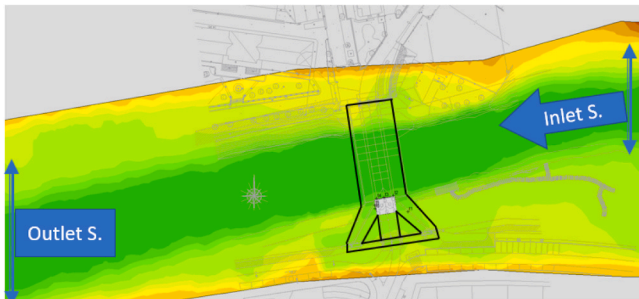


Fig. 14. Inlet and outlet (free) sections of the design flood.

these tests to collect the structural response to both tests. The specialized company responsible for instrumentation and measurement was Teknés, which produced a report with the results obtained during the tests. The following are the most relevant results from this report for the current investigation.

4.1. Static Test

The static load test consists of 7 different load configurations depending on the location of the trucks. For this article, the data from configuration 1 and configuration 2 have been used, as these analyze the bending behavior of the bridge; the others were focused on torsion

behaviour. In configuration 1 (Fig. 18), 2 rows of 4 trucks each are arranged along the main span, and 2 rows of 1 truck each along the short span, for a total of 10 trucks of approximately 260 kN. Configuration 2 is similar to configuration 1 but without placing the 2 trucks on the short span (Fig. 17b).

During the load test (Fig. 19), displacement values close to the expected ones were obtained, and the recovery of the structure's displacement was complete.

For the static load test, 10 displacement measurement devices were set up, but for the purpose of this research, only 6 of them have been used: P1, P2, P3, P4, P9, and P10 (Fig. 20a). Sensors P1 and P2 correspond to abutment 2, sensors P3 and P4 correspond to the centre of the main span, and sensors P9 and P10 are located in abutment 1. The reason for not considering sensors P5, P6, P7, and P8 is that they are placed at points with small movements, such as the pier area and the centre of the small span. With such small movements, any adjustment of the bridge during the first significant load can distort the results, whereas these effects are negligible at points with larger movements, such as the centre of the large span or the abutment area due to the neoprene supports. All of them were draw wire sensors of the SX50 series from the Waycon brand (Fig. 20b), recording values at 1 Hz. This static deflection measurement was only carried out during the execution of the static load test.

This calibration process does not require calibrating each parameter that influences the stiffness individually. If the difference from the theoretical value is not too large, it is sufficient to have a calibrated

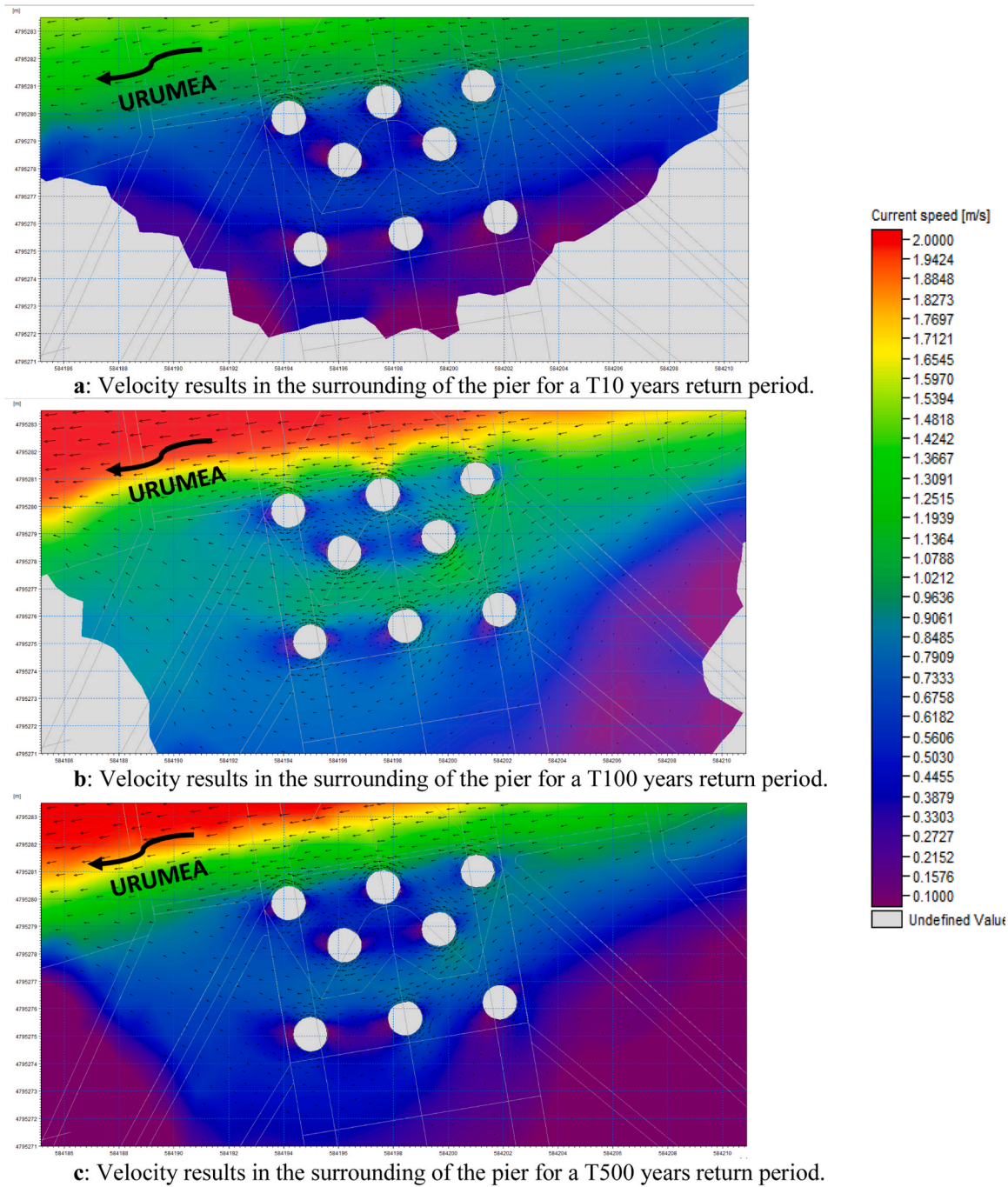


Fig. 15. (a) Velocity results in the surrounding of the pier for a T10 years return period. (b) Velocity results in the surrounding of the pier for a T100 years return period. (c) Velocity results in the surrounding of the pier for a T500 years return period.

stiffness value that averages all the parameters on which it depends.

4.2. Dynamic load test

Hypothesis of a 30 km/h speed with an amplification board.

The dynamic load test consisted of 4 hypotheses, all of them were performed with the same 260 kN truck. Two of the hypotheses were performed with the truck passing at 30 km/h, with and without amplification board (Fig. 21), and the other two were identical to the first ones, but with the truck passing at 40 km/h. For the dynamic load test, 6 triaxial accelerometers ATA-OYO AC3Tx (Fig. 22b) were used, distributed in 3 different sections (Fig. 22a) and recording at 200 Hz. These accelerometers were installed during the construction of the bridge and

were configured to continue measuring in real-time during the bridge's service phase.

In the dynamic load test, after analyzing the data from all accelerometers using the Fast Fourier Transform (FFT), a fundamental bending frequency of 2.29 Hz was obtained (Fig. 23), with an average structural damping value of 0.50 %.

4.3. Test during service phase

To characterize the bridge's behaviour under the horizontal load of regular traffic, accelerometers have continuously recorded real-time data at a frequency of 100 Hz from the opening day until the present. During the monitoring of the structure, and based on the data provided

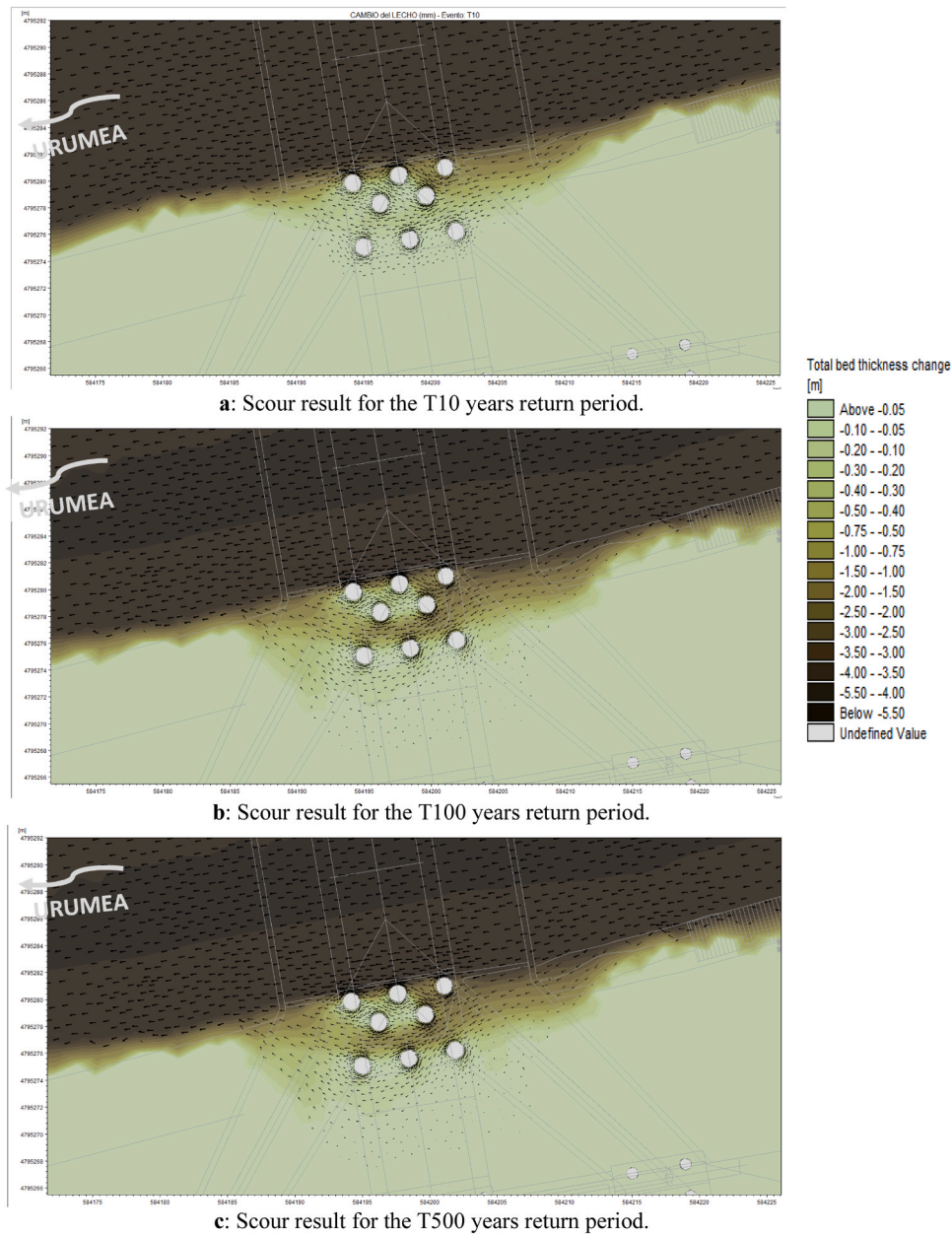


Fig. 16. (a) Scour result for the T10 years return period. (b) Scour result for the T100 years return period. (c) Scour result for the T500 years return period.

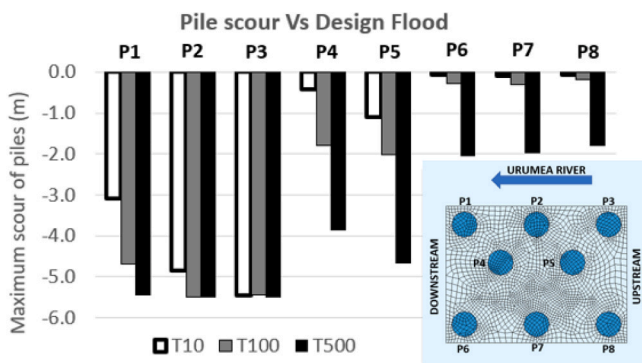


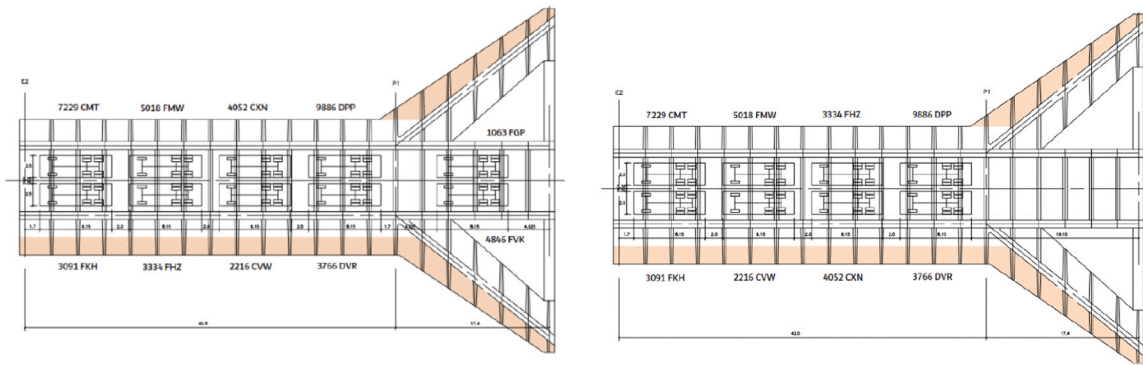
Fig. 17. Scour for each pile at the foundation of the pier of the Espartxo Bridge Vs design flood.

by the accelerometer, the frequency of 2.29 Hz obtained during the dynamic load test has remained consistent, as seen in the analysis of the data recorded on 10/11/2021 at 08:46, Fig. 24.

However, on other occasions, accelerometer data detected a frequency of 2.73 Hz, as seen in the data analyzed on 08/11/2021 at 16:53, Fig. 25.

In Fig. 24, it can be observed that at the frequency of 2.29 Hz, the horizontal component of the accelerometer is zero, meaning it is strictly a vertical movement. However, in Fig. 25, it can be identified that the horizontal component represents approximately 25% of the vertical component. In both figures, it can be observed that if one frequency appears, the other does not.

In Fig. 26, the accelerograms that allow the calculation of the frequency spectra in Fig. 24 and Fig. 25 are analysed and compared. It can be concluded that the excitation is similar in duration (a few seconds). This fact determines that the most probable cause of excitation in both accelerograms is vehicles and not another source of horizontal forces, such as the wind, for example. When analysing the data from all



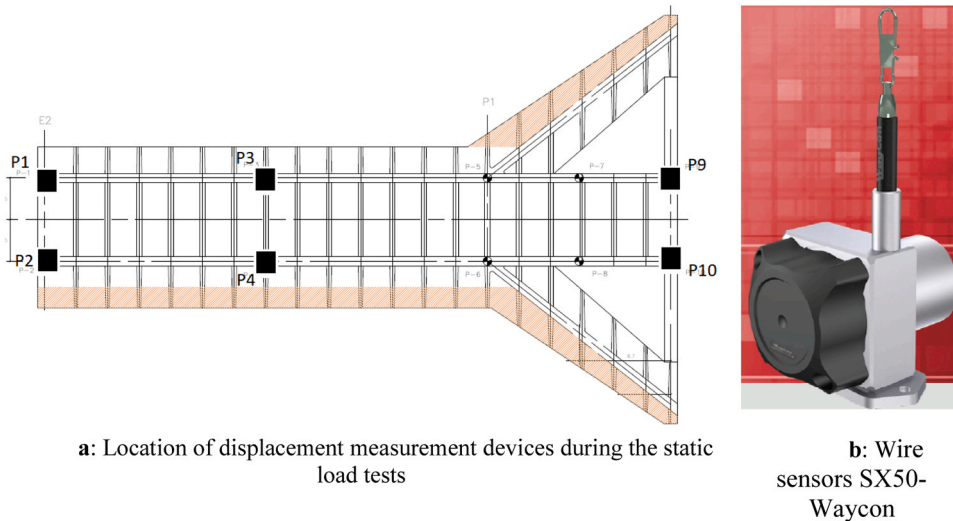
a: Static load test definition. Configuration 1. Plan View.

b: Static load test definition. Configuration 2. Plan View.

Fig. 18. (a) Static load test definition. Configuration 1. Plan View. (b) Static load test definition. Configuration 2. Plan View.



Fig. 19. Static test implementation. Configuration 2.



a: Location of displacement measurement devices during the static load tests

b: Wire sensors SX50-Waycon

Fig. 20. (a) Location of displacement measurement devices during the static load tests. (b) Wire sensors SX50-Waycon.

accelerometers, the possibility that the frequency of 2.73 Hz was associated with torsional modes was also ruled out, as the sign of the acceleration recorded by the accelerometers on each side of the span was the same. Another relevant point from this analysis, as seen in Fig. 26 by the envelope curve defining the logarithmic decrement, is that the damping is approximately double at the frequency of 2.73 Hz compared to 2.29 Hz. This could indicate that the soil is involved in the vibration mode associated with the frequency of 2.73 Hz.

Therefore, based on field data, it was concluded that the structural response of the Puente de Espartxo to horizontal forces from traffic was

influenced by soil-structure interaction and activated the frequency of 2.73 Hz, unlike when vehicle excitation was purely vertical, which activated the frequency of 2.29 Hz.

5. Finite element model of Espartxo Bridge

A finite element model (FEM) of the Espartxo bridge has been developed in the context of this research. The complex geometry of the bridge has been defined in detail. The connection between the steel longitudinal ribs and the steel transverse ribs has been modelled with



Fig. 21. Dynamic load test implementation.

accurate geometry and the appropriate eccentricity between elements. (Fig. 27).

The V-shape pier has been also modelled following its complex geometry (Fig. 28).

Firstly, the steel structure of the deck was defined with beam elements, and plate elements were arranged to generate both the roadway slab for vehicles and the slab in pedestrian areas. The pylon, which defines the central support of the deck, was modelled considering its complex geometry using beam elements. At the top of the pylon, a steel element is arranged to connect the V-shape of the pier. Additionally, the piles emerge from the pilecap as beam elements with the corresponding length (19.5 m), each with a fixed support at its tips in all three directions. To complete the finite element model, the weights of non-structural elements such as railings, the wooden pedestrian platform, steel stiffeners, and the road surface in the traffic area were added as mass. The neoprene supports on both abutments were modelled using springs with their theoretical stiffness. Two FE models were developed for this research. Firstly, a model for studying loads without a horizontal component (referred to as model 1), where there are no springs in the piles representing the soil. Secondly, an identical model but with a coefficient of subgrade reaction in the piles (referred to as model 2) for cases where there is both horizontal and vertical load.

The vibration mode of Model 1 only exhibits only vertical component in deck displacement (Fig. 29a), whereas the fundamental mode of Model 2 displays both vertical and horizontal components in deck displacement (Fig. 29b). The ratio between horizontal and vertical movement is entirely consistent with the Fig. 25. It is important to highlight that the only difference between both models is the horizontal restraint of the ground on the piles, which, in addition to inducing horizontal movement in the vibration mode, increases the vibration frequency value.

As observed when comparing the vibration modes in the upper figure, due to the lateral effect of the terrain on the piles, even if it's small, a horizontal component develops in the movement of the fundamental mode, which can be observed both in the deck and in the pile heads. This is a fundamental characteristic for this research, as will be further developed later on. It can be noticed that the ratio between vertical and horizontal movements showed in both Fig. 29a and Fig. 29b are entirely consistent with the amplitudes of the FFT shown in Fig. 24 and Fig. 25.

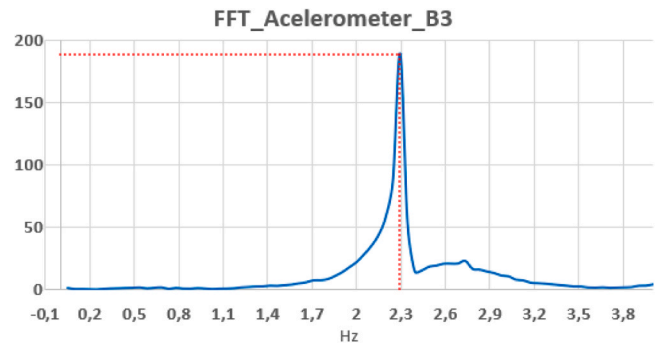


Fig. 23. Spectrum of frequencies of the bridge during the dynamic load test. Hypothesis at 30 km/h with the amplification board.

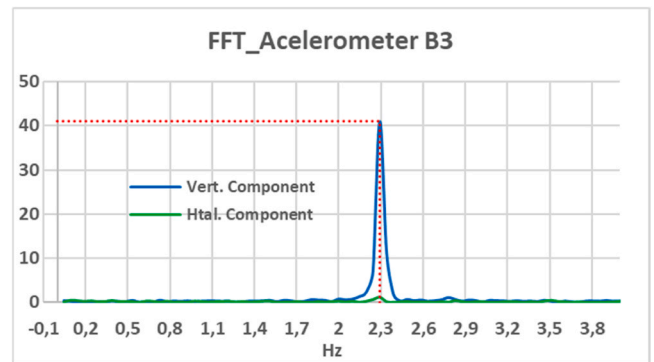
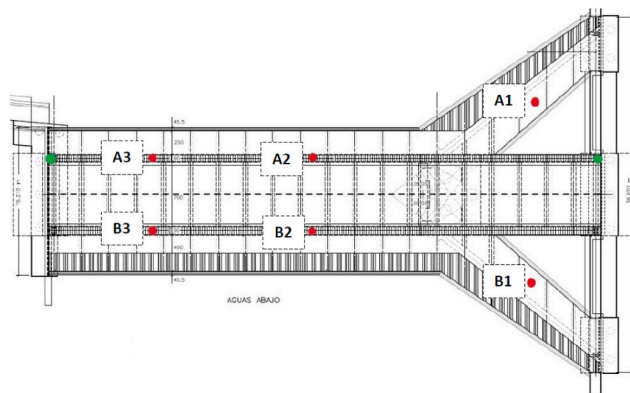


Fig. 24. Spectrum of frequencies of the bridge during the service stage.B3 accelerometer. 10/11/2021. 08:46 h.



a: Location of the accelerometers for the dynamic load tests.



b: Triaxial accelerometers ATA-OYO AC3Tx

Fig. 22. (a) Location of the accelerometers for the dynamic load tests. (b) Triaxial accelerometers ATA-OYO AC3Tx.

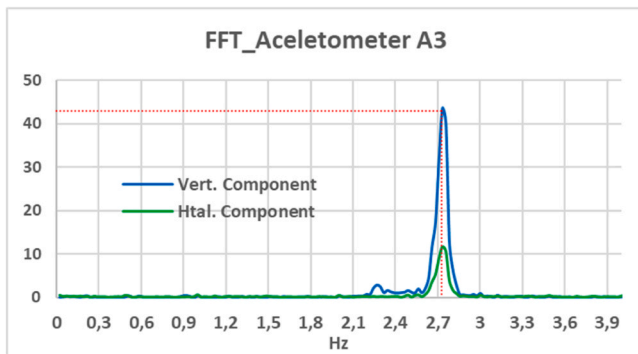


Fig. 25. Spectrum of frequencies of the bridge during the service stage.A3 accelerometer. 08/11/2021. 16:53 h.

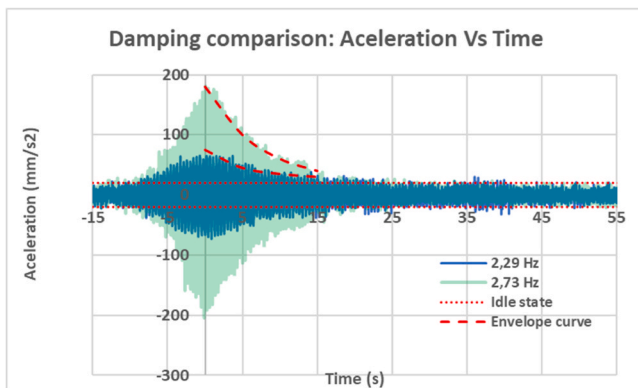


Fig. 26. Accelerograms' comparison for the frequencies of 2.29 Hz and 2.73 Hz.

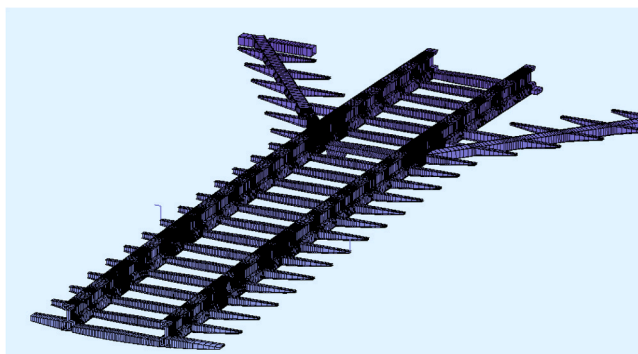


Fig. 27. Steel structure modelled at deck.

6. Twin model calibration of Espartxo Bridge

The calibration process for the stiffness, mass of the bridge, and soil-structure interaction for the twin model has been carried out independently for each variable, as explained below.

6.1. Stiffness calibration of the bridge

For the stiffness calibration of the model, different modulus of subgrade reaction values were assigned throughout the length of the pile, thus verifying if this variable influenced the displacement values. Fig. 30 shows that the maximum deflection value is practically unaffected by the subgrade reaction value, so the stiffness was calibrated with model 1.

Once confirmed that the subgrade reaction coefficient had no

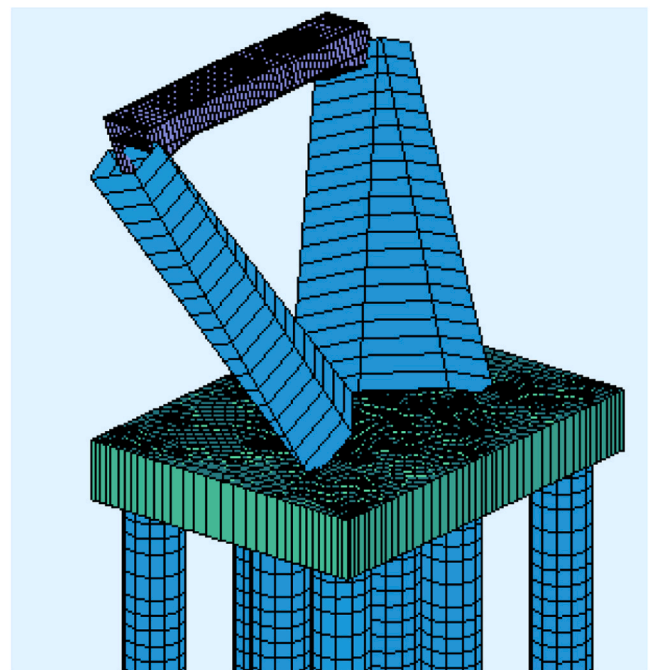


Fig. 28. Piles, pile cap and pier modelled.

influence on the vertical static displacements, configuration 1 and 2 of the static load test were modelled. The variables calibrated in the model were the vertical stiffness of the neoprene supports for movement at both abutments and the fixity level between the concrete slab and the longitudinal steel ribs due to connectors. The theoretical horizontal stiffness of the neoprenes at all supports was included in the model, but since this stiffness is negligible compared to the horizontal restraint exerted by the pile through its support in the ground, the horizontal stiffness of the neoprenes was not included as a calibration parameter. With minor adjustments to the vertical neoprene's stiffness and the level of fixity between the slab and longitudinal rib, it was possible to replicate both configuration 1 (Fig. 31a) and configuration 2 (Fig. 31b) of the static load test. The numerical values are presented in Table 5.

6.2. Mass calibration of the bridge

The participation of masses in the deck) is the one with the greatest influence on the vibration modes studied in this research. Therefore, for the mass calibration, only the mass of the deck has been modified. In Fig. 32, the variation of the natural vibration frequency of model 1 can be observed as a function of the variation in the theoretical value of the deck mass, including non-structural masses. With a 1.2 % increase in the deck mass over the theoretical value, a frequency of 2.29 Hz is obtained, as shown in Fig. 31.

6.3. Soil-pier interaction calibration

Once the bridge's stiffness and mass have been calibrated, the next step is to calibrate the soil stiffness. To achieve this, the theoretical values of the horizontal coefficient of subgrade reaction defined in Section 3.2 are multiplied by a soil factor of 0.98 to obtain the measured frequency of 2.73 Hz, as shown in Fig. 33.

7. Numerical analysis of the scour of Espartxo Bridge

Once the model is calibrated, it serves as a very useful tool for detecting scour due to its sensitivity to changes in vibration modes with a horizontal component [31]. For this reason, once the twin model of the bridge has been developed, an analysis has been performed to determine

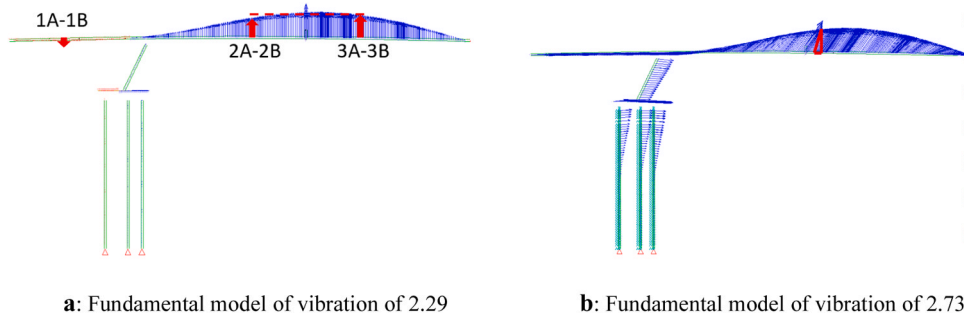


Fig. 29. (a) Fundamental model of vibration of 2.29 Hz. Without horizontal motion component (Model 1). (b) Fundamental model of vibration of 2.73 Hz. With horizontal movement component (Model 2).

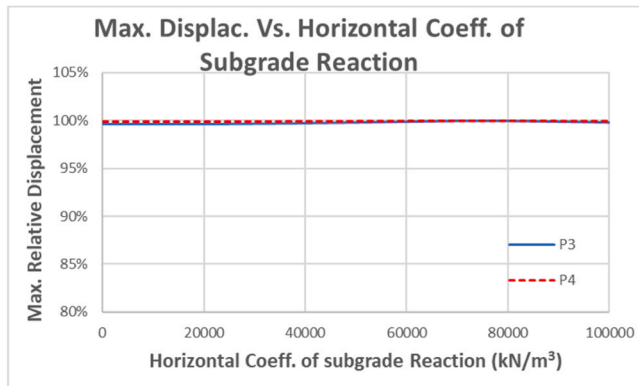


Fig. 30. Maximum relative displacement of the centre of the main span Vs. Coefficient of subgrade reaction.

the correlation between possible scouring of the soil under the pile and the natural vibration frequency of 2.73 Hz. To achieve this, the springs modelling the soil restraint on each pile have been progressively removed according to the study conducted in Section 3.3 of this document, as shown in Fig. 34. With the modification of the horizontal soil restraint for each design flood event, dynamic analyses have been performed in model 2 to determine the variation in vibration frequency with this new configuration. Some authors recommend considering the influence of changes in soil properties under scour due to the loss of material from the upper layers [32]. However, in this case, scour is not understood as a total loss of the upper layers of soil but as a localized loss around the piles, so that effect has not been considered in the calculations.

The influence of the scour has been analyzed at the frequency of 2.73 Hz for the three-design flood of 10 years, 100 years and 500 years, Fig. 35.

Table 5 Model values and load test comparison.

Check point	Configuration 1		Configuration 2	
	Model	Load test	Model	Load test
P1-P2	-0,13	-0,18	-0,13	-0,18
P3-P4	-2,58	-2,58	-2,66	-2,74
P9-P10	0,01	0,02	0,03	0,05

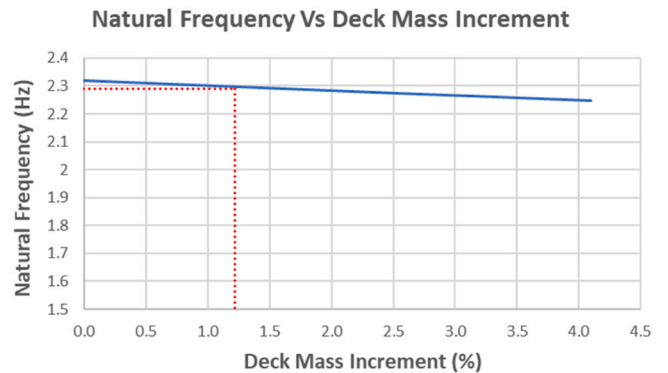
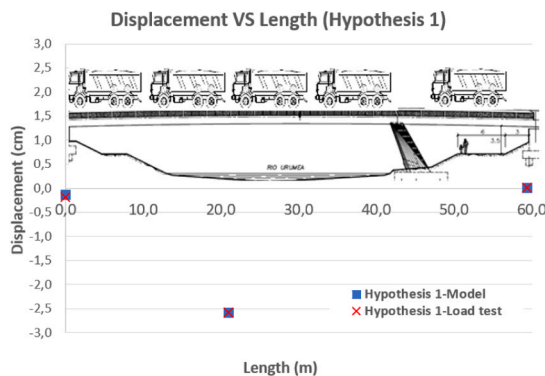
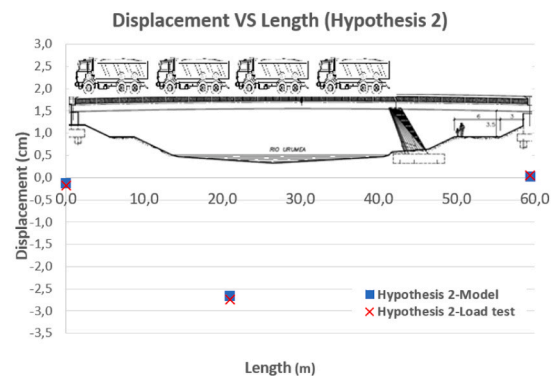


Fig. 32. Natural frequency of vibration Vs. Increment of mass of the deck from the theoretical value.



a: Configuration 1. Model Vs. Load test.



b: Configuration 2. Model Vs. Load test.

Fig. 31. (a) Configuration 1. Model Vs. Load test. (b) Configuration 2. Model Vs. Load test.

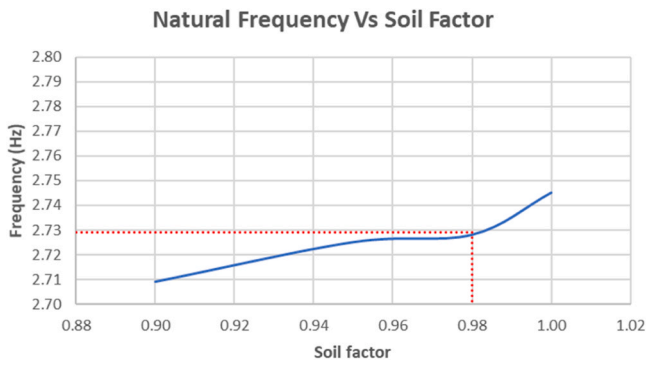


Fig. 33. Frequency of vibration Vs Calibration of soil factor.

The Fig. 35 shows the average scour depth of the piles grouped in rows: the row of piles closest to the Urumea River (P1-P2-P3), the middle row (P4-P5), the innermost row (P6-P7-P8), and the combined average of the three rows. It can be observed that a 10-year flood, which is highly likely during the structure’s lifespan, despite causing significant scour predominantly in the more exposed row of piles, substantially alters the natural frequency to a value of 2.62 Hz. The 100-year design flood induces scour up to the middle row of piles, but the frequency is not excessively affected, 2.60 Hz. The 500-year flood, with significant, albeit uneven scour in all three rows of piles, reduces the vibration frequency to 2.55 Hz. These results, coupled with the real-time monitoring of the bridge through the deployed instrumentation, enable the establishment of a preventive alarm based on the frequency values to detect potential scouring beneath the foundation. Any defect that might reduce the stiffness of the deck, the pier, or the foundation would cause a variation in both the 2.29 Hz and 2.73 Hz frequencies. However, if only the frequency of 2.73 Hz is affected, then necessarily, the frequency variation must be caused by the lack of support from the soil, as it is the only difference between the developed calibrated FE models. Therefore, this research would allow the establishment of an alarm for the risk of scouring with a very high level of confidence. In addition to the frequency analysis, the increase in internal forces on the piles due to

horizontal forces has been studied based on the level of scouring. The analysis was performed at the pile head section, as it is the critical section, as shown in Fig. 36a. The relative increase in bending moment due to horizontal loads, depending on the level of scouring reached, is presented in Fig. 36b. The maximum results for each group of pile rows are shown. As observed in the figure, the piles most affected are those in the row farthest from the Urumea River, where bending moments can increase by almost 30 % for the scouring level corresponding to the 500-year flood.

8. Conclusions of Espartxo Bridge

A digital twin of the Espartxo Bridge has been developed, enabling predictive maintenance on the structure. Specifically, in this article, the digital twin has been applied for early detection of undermining in the bridge’s foundation, as it has been documented as the primary cause of bridge collapses worldwide.

To achieve this, a geotechnical study of the terrain on which the bridge is founded was conducted, along with a hydraulic study to determine the torrential flows associated with project design floods, assessing their potential for undermining. Real load tests were also performed on the bridge, including both static and dynamic tests. With all the available information, all necessary parameters for the digital twin were independently calibrated, including the horizontal restraint of the soil on the piles. For this latter parameter, data from instrumentation during actual service conditions, i.e., under the loads of real traffic, were analyzed, as the Espartxo Bridge is continuously monitored in real-time. After this analysis, the vibration frequency activated during vehicle braking, with a value of 2.73 Hz, and the fundamental frequency activated under exclusively vertical traffic loads, with a value of 2.29 Hz, have been identified. The vibration mode associated with the frequency of 2.29 Hz is activated when vehicles do not transmit horizontal loads, and therefore, the bridge does not require support from the soil. On the other hand, the mode associated with the frequency of 2.73 Hz is activated when, due to the horizontal loads transmitted by traffic, the bridge, through its piles, laterally supports itself on the soil. Based on this difference in the boundary conditions of the bridge according to the type of loading, the horizontal restraint exerted by the soil on the piles

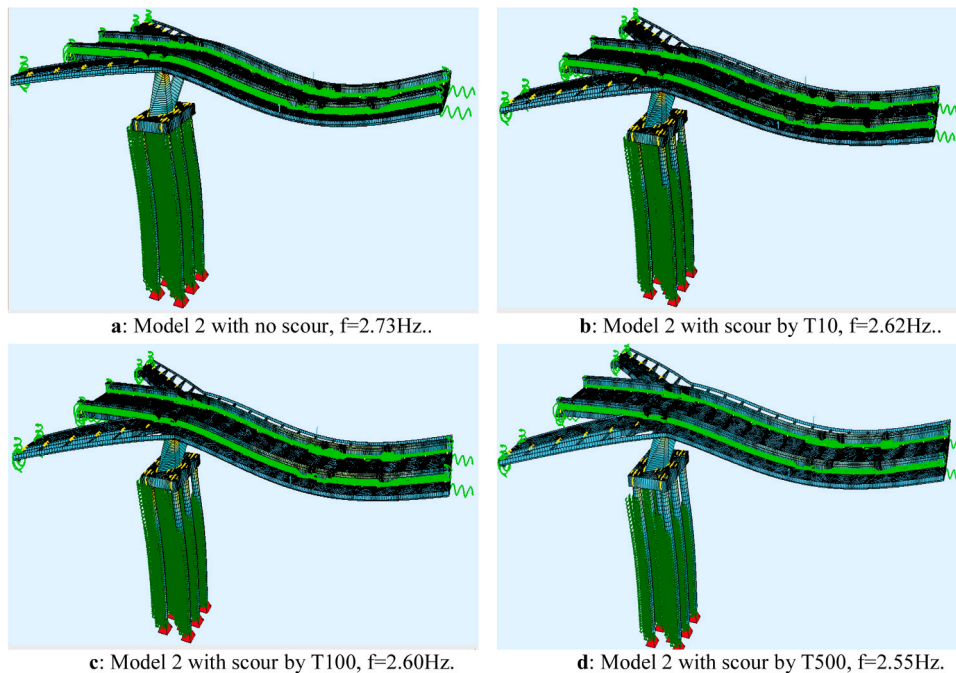


Fig. 34. (a) Model 2 with no scour, $f = 2.73$ Hz. (b) Model 2 with scour by T10, $f = 2.62$ Hz. (c) Model 2 with scour by T100, $f = 2.60$ Hz. (d) Model 2 with scour by T500, $f = 2.55$ Hz.

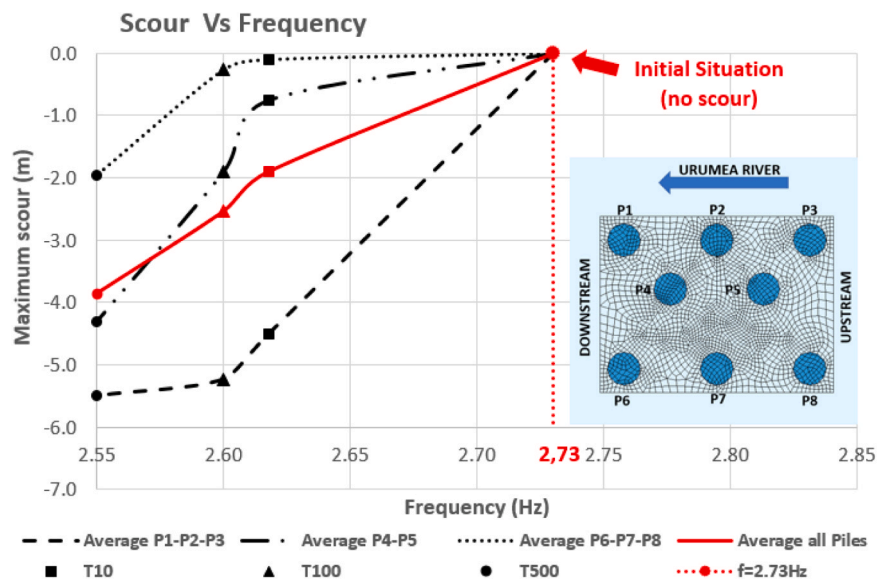


Fig. 35. Average scour of row piles Vs. Frequency of vibration of the bridge.

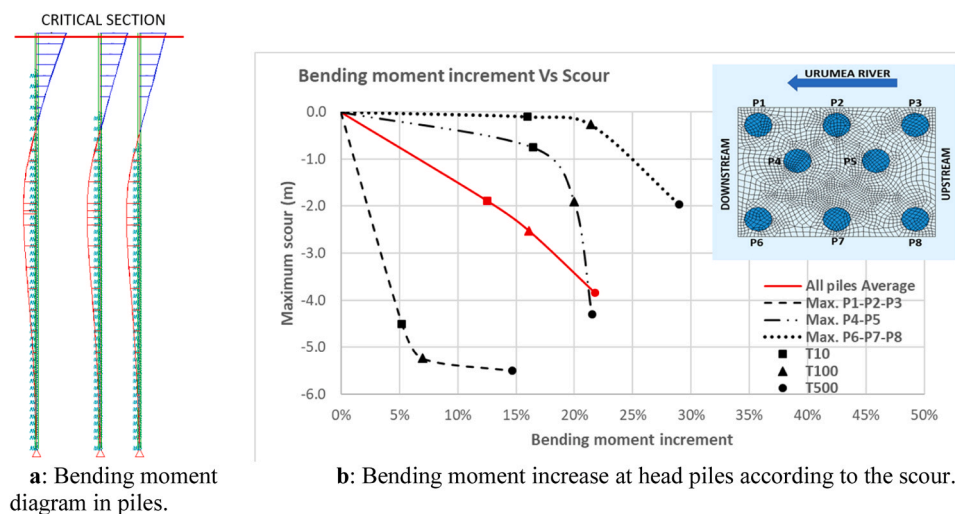


Fig. 36. (a) Bending moment diagram in piles. (b) Bending moment increase at head piles according to the scour.

has been independently calibrated from the rest of the parameters. Once the digital twin of the Espartxo bridge has been developed and calibrated in its baseline condition, the horizontal restraint of the soil has been modified according to the pile scour obtained from the torrential flow study for the 10-year, 100-year, and 500-year return period floods. For each studied scour condition, a dynamic analysis has been performed to establish the correlation between the isolated variation of the 2.73 Hz frequency and the depth of scour. Finally, it has been demonstrated that scour substantially increases the forces in the piles farthest from the river under horizontal loads, posing structural risks both in terms of strength and durability. In conclusion, it can be inferred that the level of scour that could occur in the first meters of the piles beneath the pier of the Espartxo Bridge could be unequivocally detected if there is a decrease in the vibration frequency of 2.73 Hz while keeping the frequency of 2.29 Hz constant. Both frequencies can be measured in real-time by the accelerometers installed on the bridge. Consequently, it is possible to establish an instant alarm based on the measured values in the structural monitoring instrumentation of the bridge. This preventive measure can help avoid structural issues in the bridge resulting from the scouring process, a factor that has caused numerous collapses in structures throughout the recent history of bridges.

CRedit authorship contribution statement

Marianela García: Methodology, Project administration, Software. **Javier Sanchez-Haro:** Conceptualization, Data curation, Formal analysis, Investigation, Methodology, Software, Writing – original draft, Writing – review & editing. **Guillermo Capellán:** Conceptualization, Funding acquisition, Resources, Supervision, Validation. **Paula Perez:** Data curation, Software, Writing – original draft. **Almudena da Costa:** Formal analysis, Investigation, Writing – original draft, Writing – review & editing. **Javier Año:** Data curation, Software.

Declaration of Competing Interest

The authors declare that they have no known competing financial interests or personal relationships that could have appeared to influence the work reported in this paper.

Aknowledgments

This research has been made possible thanks to the support of the City Council of San Sebastián, the company Arenas & Asociados, the

Juan José Arenas Chair at the University of Cantabria, Teknés, and FJA Ingenieros.

References

- [1] Cook W, Barr PJ, Halling MW. Bridge failure rate. *J Perform Const Facil* 2015;29(3):04014080. [https://doi.org/10.1061/\(ASCE\)CF.1943-5509.0000571](https://doi.org/10.1061/(ASCE)CF.1943-5509.0000571).
- [2] Wardhana K, Hadipriono FC. Analysis of recent bridge failures in the United States. *J Perform Const Facil* 2003;17(3):144–50. [https://doi.org/10.1061/\(ASCE\)0887-3828\(2003\)17:3\(144\)](https://doi.org/10.1061/(ASCE)0887-3828(2003)17:3(144)).
- [3] Schaap HS, Caner A. Bridge collapses in Turkey: causes and remedies. *Struct Infrastruct Eng* 2022;18(5):694–709. <https://doi.org/10.1080/15732479.2020.1867198>.
- [4] Dutta SC, Roy R. A critical review on idealization and modeling for interaction among soil–foundation–structure system. *Comp Struct* 2002;80(20-21):1579–94. [https://doi.org/10.1016/S0045-7949\(02\)00115-3](https://doi.org/10.1016/S0045-7949(02)00115-3).
- [5] Williams P, Balachandrar R, Bolisetti T. Effect of densimetric Froude number on local bridge pier scour. *International Conference on Scour and Erosion*. Oxford; 2016. (<http://eprints.hrwallingford.com/id/eprint/1182>).
- [6] Li J, Zhang B, Shen C, Fu X, Li W. Experimental study on local scour depth around monopile foundation in combined waves and current. *Sustainability* 2021;13:13614. <https://doi.org/10.3390/su132413614>.
- [7] Mohamed YA, Nasr-Allah TH, Abdel-Aal GM, Awad AS. Investigating the effect of curved shape of bridge abutment provided with collar on local scour, experimentally and numerically. *Ain Shams Eng J* 2015;6:403–11. <https://doi.org/10.1016/j.asej.2014.10.011>.
- [8] Prendergast LJ, Hester D, Gavin K, O'Sullivan JJ. An investigation of the changes in the natural frequency of a pile affected by scour. *J Sound Vibrat* 2013;332:6685–702. <https://doi.org/10.1016/j.jsv.2013.08.020>.
- [9] Bouja N, Schmidt F, Siegert D, Bang DPVan, Chevalier C. Modelling of a bridge pier subjected to scour. *Procedia Eng* 2017;199:2925–30. <https://doi.org/10.1016/j.proeng.2017.09.343>.
- [10] Foti S, Sabia D. Influence of foundation scour on the dynamic response of an existing bridge. *J Bridge Eng* 2011;16(2):295–304. [https://doi.org/10.1061/\(ASCE\)BE.1943-5592.0000146](https://doi.org/10.1061/(ASCE)BE.1943-5592.0000146).
- [11] Bao T, Liu Z. Vibration-based bridge scour detection: a review. *Struct Control Health Monit* 2016;1–19. <https://doi.org/10.1002/stc.1937>.
- [12] Maroni A, Tubaldi E, Ferguson N, Tarantino A, McDonald H, Zonta D. Electromagnetic sensors for underwater scour monitoring. *Sensors* 2020;20:4096. <https://doi.org/10.3390/s20154096>.
- [13] Prendergast LJ, Gavin K. A review of bridge scour monitoring techniques. *J Rock Mech Geotech Eng* 2014;6:138–49. <https://doi.org/10.1016/j.jrmge.2014.01.007>.
- [14] Galvin P, Dominguez J. Dynamic analysis of a cable stayed deck steel arch bridge. *J Constr Steel Res* 2007;63:1024–35. <https://doi.org/10.1016/j.jcsr.2006.11.001>.
- [15] Ballio F, Ballio G, Franzetti S, Crotti G, Solari G. Actions monitoring as an alternative to structural rehabilitation: case study of a river bridge. *Struct Control Health Monit* 2018;25:e2250. <https://doi.org/10.1002/stc.2250>.
- [16] Prendergast LJ, Hester D, Gavin K. Determining the presence of scour around bridge foundations using vehicle-induced vibrations. *J Bridge Eng* 2016;21(10):04016065. [https://doi.org/10.1061/\(ASCE\)BE.1943-5592.0000931](https://doi.org/10.1061/(ASCE)BE.1943-5592.0000931).
- [17] Maroni A, Tubaldi E, Val DV, MacDonald H, Zonta D. Using Bayesian networks for the assessment of underwater scour for road and railway bridges. *Struct Health Monit* 2020;20(5):2446–60. <https://doi.org/10.1177/1475921720956579>.
- [18] Najafzadeh M, Barani G, Hessami-Kermani M. Evaluation of GMDH networks for prediction of local depth at bridge abutments in coarse sediments with thinly armored beds. *Ocean Eng* 2015;104:387–96. <https://doi.org/10.1016/j.oceaneng.2015.05.016>.
- [19] Mohammed YA, Saleh YK, Ali AM. Experimental investigation of local scour around multi-vents bridge piers. *Alex Eng J* 2015;54:197–203. <https://doi.org/10.1016/j.aej.2015.03.004>.
- [20] Scozzese F, Ragni L, Tubaldi E, Gara F. Modal properties variation and collapse assessment of masonry arch bridges under scour action. *Eng Struct* 2019;199:109665. <https://doi.org/10.1016/j.engstruct.2019.109665>.
- [21] Tubaldi E, Macorini L, Izzuddin BA, Manes C, Laio F. A framework for probabilistic assessment of clear-water scour around bridge piers. *Struct Saf* 2017;69:11–22. <https://doi.org/10.1016/j.strusafe.2017.07.001>.
- [22] Yu P, Zhu L. Numerical simulation of local scour around bridge piers using novel inlet turbulent boundary conditions. *Ocean Eng* 2020;218:108166. <https://doi.org/10.1016/j.oceaneng.2020.108166>.
- [23] Capellan G, Garcia M, Sacristan M, Godoy A, Berrazueta JD. Diseño y construcción del nuevo Puente de Espartaco sobre el río Urumea, San Sebastián. *Horm Y Acero* 2023. <https://doi.org/10.33586/hya.2020.2838>.
- [24] Terzaghi K. Evaluation of coefficients of subgrade reaction. *Geotechnique* 1955;5(4):297–329.
- [25] Reese LC, Cox WR, Koop FD. Analysis of laterally loaded pile in sand. *Proc 6th Annu Offshore Tech Conf* 1974:473–83.
- [26] Davisson MT. Lateral load capacity of piles. *Hig Res Rec* 1970;333:104–12.
- [27] S. Prakash, "Behaviour of pile groups subjected to lateral loads" Ph.D. thesis, Univ. of Illinois, Urbana, 1962.
- [28] Jampel S. An analysis of groups of piles, I, II. no. 8, pp. 253–257 *Concr Constr Eng* 1949;44(7):201–8. no. 8, pp. 253–257.
- [29] W.W. Chen Discussion: Laterally loaded piles: Program Documentation JGED, ASCE, GT1 1978 161 162.
- [30] Zhang L, Einstein HH. Using RQD to estimate the deformation modulus of rock masses. *Int J Rock Mech Min Sci* 2004;41:337–41. [https://doi.org/10.1016/S1365-1609\(03\)00100-X](https://doi.org/10.1016/S1365-1609(03)00100-X).
- [31] Elsaid A, Seracino R. Rapid assessment of foundation scour using the dynamic features of bridge superstructure. *Constr Build Mat* 2014;50:42–9. <https://doi.org/10.1016/j.conbuildmat.2013.08.079>.
- [32] Lin C, Bennett C, Han J, Parson RL. Scour effects on the response of laterally loaded piles considering stress history of sand. *Compt Geotech* 2010;37(7-8):1008–14. <https://doi.org/10.1016/j.compgeo.2010.08.009>.